Analysis of a Supersonic Inlet Using 2D Steger-Warming and Roe Schemes

MAE250D – Computational Aerodynamics

August 27, 2021

Alexandre Law

1 Introduction

In aerospace, there are multitudes of propulsion methods that are used to achieve supersonic speeds. One common engine that is used to achieve supersonic speed is a ramjet. A ramjet operates at high speeds by taking in the freestream air and compressing the air prior to combustion. This creates a high-pressure zone that can create better combustion and ultimately more thrust.

The goal of this project is to solve the flow properties of a 2-D supersonic engine inlet problem. For this problem, we are given the engine inlet geometry and the freestream flow conditions. The two methods used to solve the 2D Euler Equation are the Steger-Warming scheme and the Roe scheme.

While a ramjet is typically axis-symmetric, we are performing our CFD analysis on a 2-D cross-section near the inlet shown below.
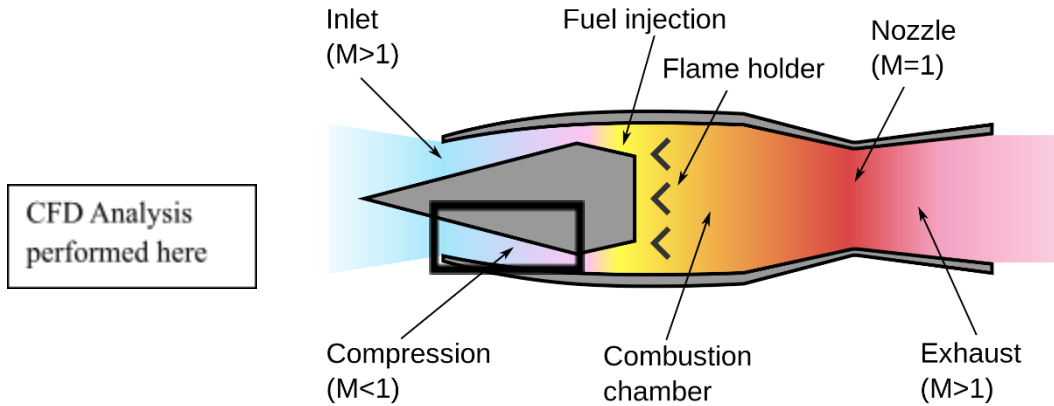

Figure 1 – Supersonic Ramjet

2 Governing Equations

We begin with our governing 2-D Euler Equations:

$$\frac{\partial U}{\partial t} + \nabla \cdot \vec{F} = 0$$

(1)

$$\vec{F} = E\vec{i} + F\vec{j}$$

(2)

Where U is the conservative variables and E and F comprise the flux vectors:

$$U = \begin{bmatrix} \rho \\ \rho u \\ \rho v \\ e \end{bmatrix} \qquad E = \begin{bmatrix} \rho u \\ \rho u^2 + p \\ \rho u v \\ (e+p)u \end{bmatrix} \qquad F = \begin{bmatrix} \rho v \\ \rho u v \\ \rho v^2 + p \\ (e+p)v \end{bmatrix}$$

(3)

Density is defined by the variable ρ, the horizontal component of velocity is defined by the variable u, the vertical component of velocity is defined by the variable v, pressure is defined by p, and e is the total internal energy per unit volume.

For a perfect gas, we determine the total internal energy by (4). γ is the ratio of specific heats.

$$\Rightarrow e = \rho c_v T + \frac{\rho}{2}\left(u^2 + v^2\right)$$

$$= \frac{p}{\gamma - 1} + \frac{\rho}{2}\left(u^2 + v^2\right), \qquad \gamma = \frac{c_p}{c_v}$$

(4)

3 Geometry and Exact Solution

The geometry of our supersonic inlet is shown in Figure 2. The inlet itself is characterized by a short straight section that hits a straight tapered section all the way to the exit. The intersecting lines approximate the oblique shockwave locations, and the numbered sections correspond to the main flow sections of interest. The upper wall angle and initial oblique shock angle are given as $\theta = 10.94°$ and $\beta = 29°$.
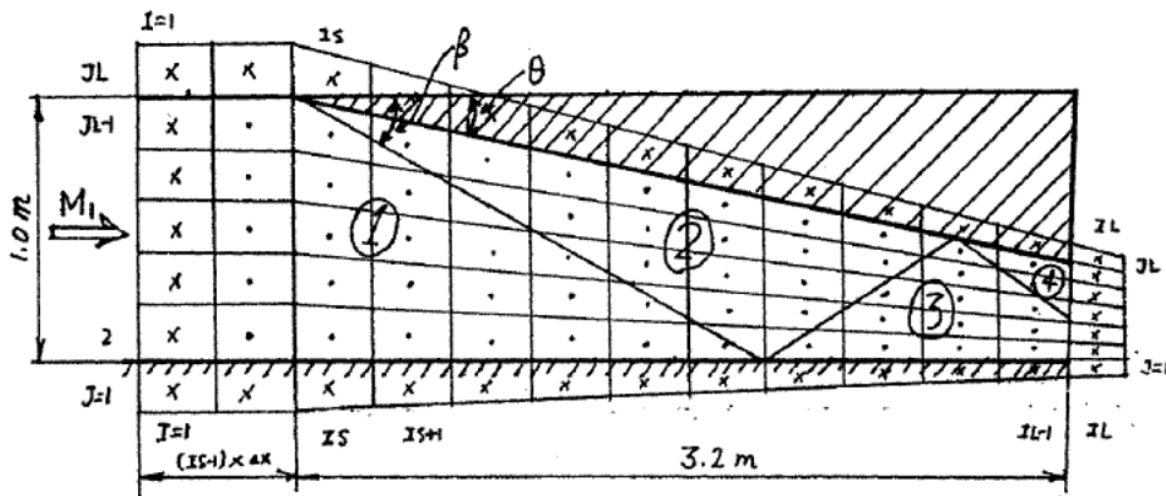
Figure 2 – Supersonic Inlet Geometry

To verify the accuracy of computation, the theoretical exact solutions are given in table 1 as comparison.

Section	M (Mach Number)	Pressure (N/m^2)
1	2.9	10^5
2	2.378	2.141 x 10^5
3	1.942	4.109 x 10^5
4	1.551	7.287 x 10^5

Table 1 – Exact Solutions

Section 4 Boundary Conditions

The inlet boundary conditions are given in Section 1. At the inlet the flow is supersonic with a Mach Number = 2.9.

The top and bottom walls of the domain maintain a no flow through condition so the normal component of velocity at the wall equals 0.

The treatment of the boundary cells is given with a simple extrapolation formula. Each slave cell will adopt the properties of its neighboring non-slave cell control volume after each iterative loop. This is exemplified in equation set (5) where the conservative variables [U] are adopted by the slave cells. The format of the below pseudo-code is f(rows, columns).

$$\text{Top wall: U(JL, :) = U(JL-1, :)}$$

$$\text{Bottom wall: U(1, :) = U(2, :)}$$

(5)

$$\text{Inlet: U(:, 1) = U(:, 2)}$$

$$\text{Exit: U(:, IL) = U(:, IL-1)}$$

Section 5 Finite Volume Method

The Euler equation (1) is integrated with a volume integral to obtain equation (6).

$$\int_V \frac{\partial U}{\partial t} dV + \int_V \left(\nabla \cdot \vec{F} \right) dV = 0$$

(6)

Applying the divergence theorem to the second term yields equation (7).

$$\int_V \left(\nabla \cdot \vec{F} \right) dV = \int_S \vec{F} \cdot d\vec{s} = \int_S \vec{F} \cdot \vec{n} \, ds$$

(7)

Next, we pull the *dt* out of the first term because the cell volume remains constant over time. The second term is rewritten with a surface integral as we are evaluating the net flux terms across the boundary of each cell. Equation (7) can be written as (8).

$$\frac{\partial}{\partial t}\int_V U dV + \oint_S \vec{F} \cdot d\vec{s} = 0$$

(8)

We define the cell average as equation (9).

$$\overline{U}_{ij} = \frac{\int_V U dV}{V_{ij}}$$

(9)

Inserting this back into equation (8) and the entire equation by $1/(V_{ij})$ we obtain equation (10).

$$\frac{\partial \overline{U}_{ij}}{\partial t} + \frac{1}{V_{ij}}\oint_S \vec{F} \cdot d\vec{s} = 0$$

(10)

This leads us to our general formulation which we base our two schemes off. The surface integral in the second term can be rewritten as the sum of the flux terms across each boundary wall. This is denoted by the subscript *i ±½* and *j ±1/2* in equation (11).

$$\frac{\partial \overline{U}_{ij}}{\partial t} = -\frac{1}{V_{ii}}\left[\left(\vec{F} \cdot d\vec{s}\right)_{i+1/2} + \left(\vec{F} \cdot d\vec{s}\right)_{i-1/2} + \left(\vec{F} \cdot d\vec{s}\right)_{j+1/2} + \left(\vec{F} \cdot d\vec{s}\right)_{j-1/2}\right]$$

(11)

Section 6 Steger-Warming and Roe Scheme

For the purposes of space and clarity, only the top-level equations for the Steger-Warming (Section 7) and Roe (Section 8) scheme will be provided. The equations and description of each variable can be found in the lecture notes.

The finite volume formulation is given in equation (12).

$$\frac{\partial \overline{U}_{ij}}{\partial t} + \frac{1}{V_{ij}}\left[\left(E''_{i+1/2}S_{i+1/2} - E''_{i-1/2}S_{i-1/2}\right) + \left(F''_{j+1/2}S_{j+1/2} - F''_{j-1/2}S_{j-1/2}\right)\right] = 0$$

(12)

The computation equation for the Steger-Warming approximation scheme is given by equation (13).

$$\overline{U}_{ij}^{n+1} = \overline{U}_{ij}^{n} - \frac{\Delta t}{V_{ij}} \left\{ \left[\overbrace{E_{i+1/2}^{S-W}\left(\text{use } n_{x_{i+1/2}} \ n_{y_{i+1/2}}\right)}^{} \atop \left(E_{i+1j}^{"-"} + E_{ij}^{"+"}\right) S_{i+1/2} - \left(E_{ij}^{"-"} + E_{i-1j}^{"+"}\right) S_{i-1/2} \right] \right.$$

$$\left. + \left[\overbrace{F_{j+1/2}^{S-W}}^{} \atop \left(F_{ij+1}^{"-"} + F_{ij}^{"+"}\right) S_{j+1/2} - \left(F_{ij}^{"-"} + F_{ij-1}^{"+"}\right) S_{j-1/2} \right] \right\} = 0 \qquad (13)$$

Similarly, the Roe scheme is given in equation (14).

$$U_{ij}^{n+1} = U_{ij}^{n} - \frac{\Delta t}{V_{ij}} \left\{ \left(E''^{n\,(\text{Roe})}_{\ i+1/2} \ S_{i+1/2} - \left(E''^{n\,(\text{Roe})}_{\ i-1/2}\right) S_{i-1/2} \right) \right.$$

$$\left. + \left(F''^{n\,(\text{Roe})}_{\ j+1/2} \ S_{j+1/2} - \left(F''^{n\,(\text{Roe})}_{\ j-1/2}\right) S_{j-1/2} \right) \right\} \qquad (14)$$

Section 7 Grid Generation

Table 2 provide the grid densities used in this analysis. JL represents the number of discretized cell-volumes in the vertical (y) direction and IL represents the horizontal (x) direction.

	IL	JL
Grid #1	42	22
Grid #2	82	42
Grid #3	162	82

Table 2 – Grid Density

The three grids are displayed in Figures 3, 4, and 5.

The grid itself was generated using the differential method. The initial cells were determined by the algebraic method. Where the entire domain was divided uniformly in the x and y directions. The perimeter cells denoted by an x in Figure 2 represent the slave cells. The purpose of the slave cells is to allow the computation of our interior cell volumes without special boundary treatments (i.e. one-sided finite volume). This simplifies the overall computational program with minimal loss in accuracy.
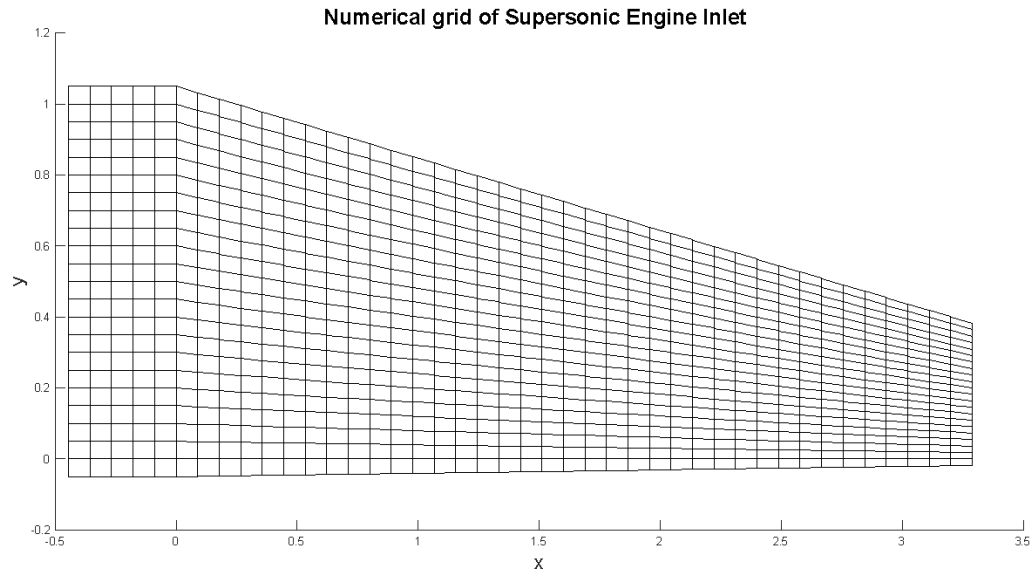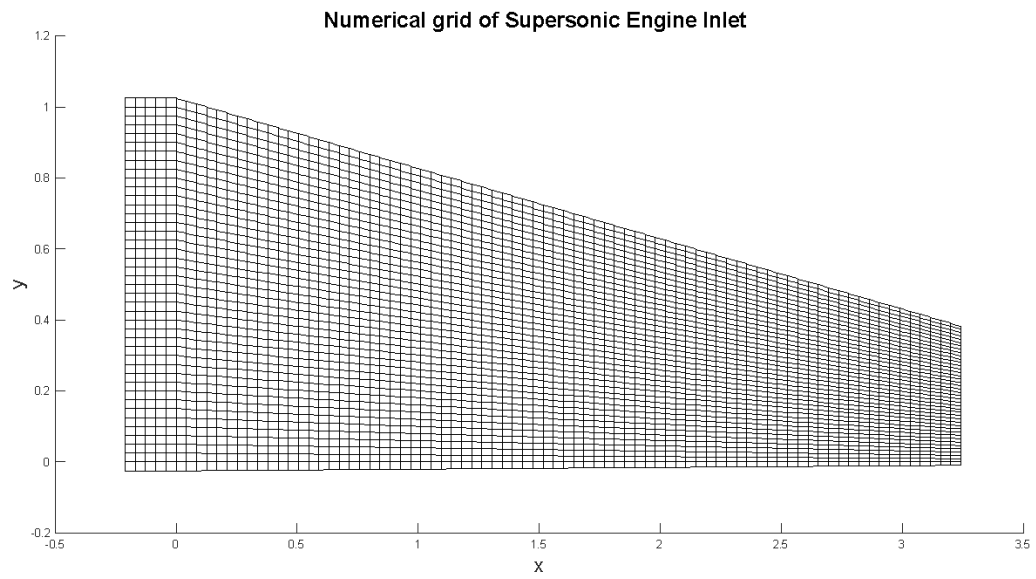
Figure 3: Grid Generation for IL = 42, JL = 22

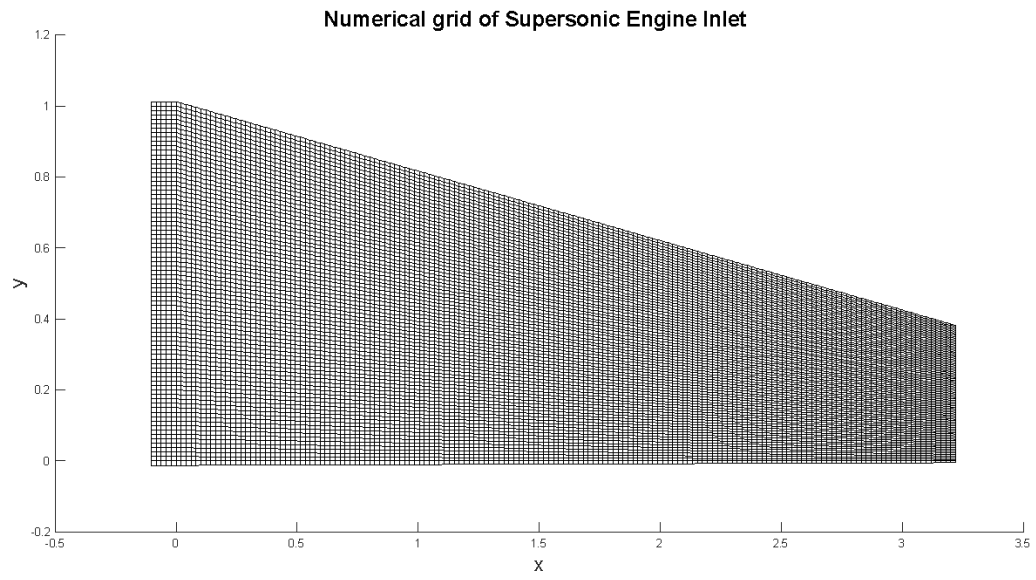Figure 4: Grid Generation for IL = 82, JL = 42

Figure 5: Grid Generation for IL = 162, JL = 82

Section 7 Results

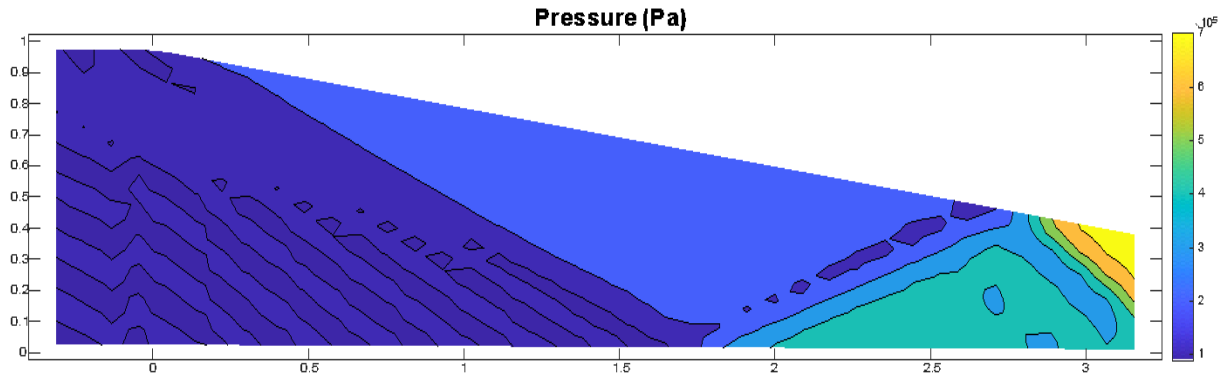Shown are plots utilizing MacCormack Method

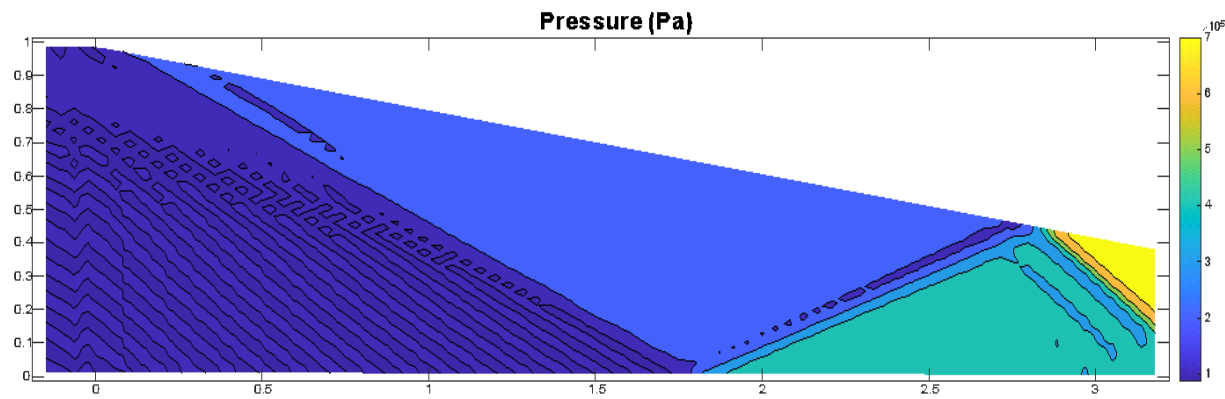Figure 6 – Contour plot for pressure at IL = 42, JL = 22

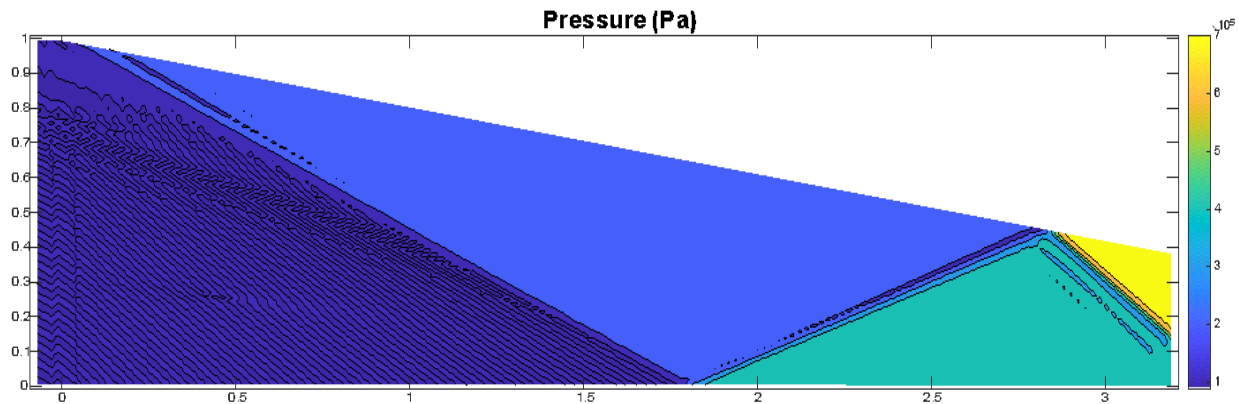Figure 7 – Contour plot for pressure at IL = 82, JL = 42

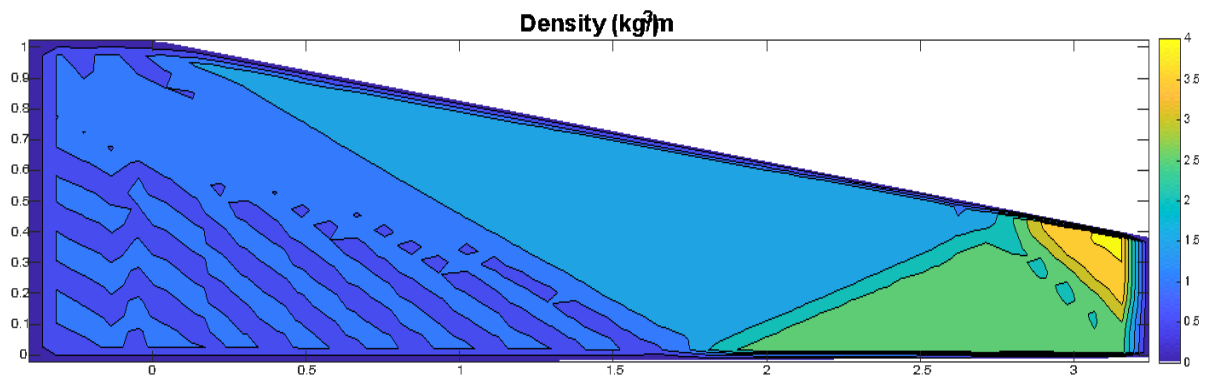Figure 8 – Contour plot for pressure at IL = 162, JL = 82
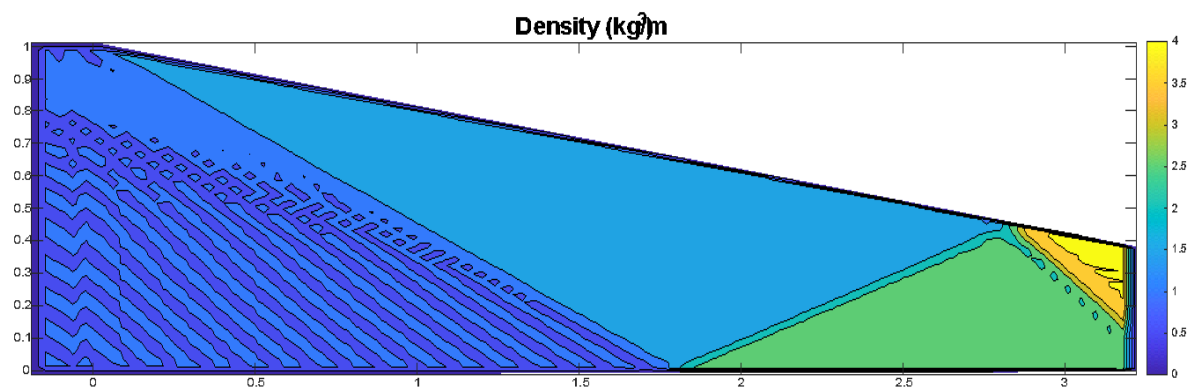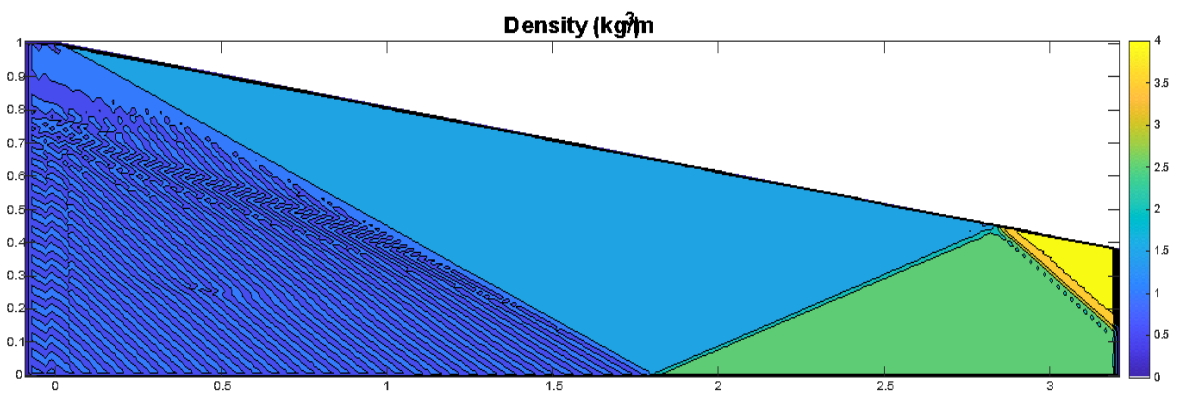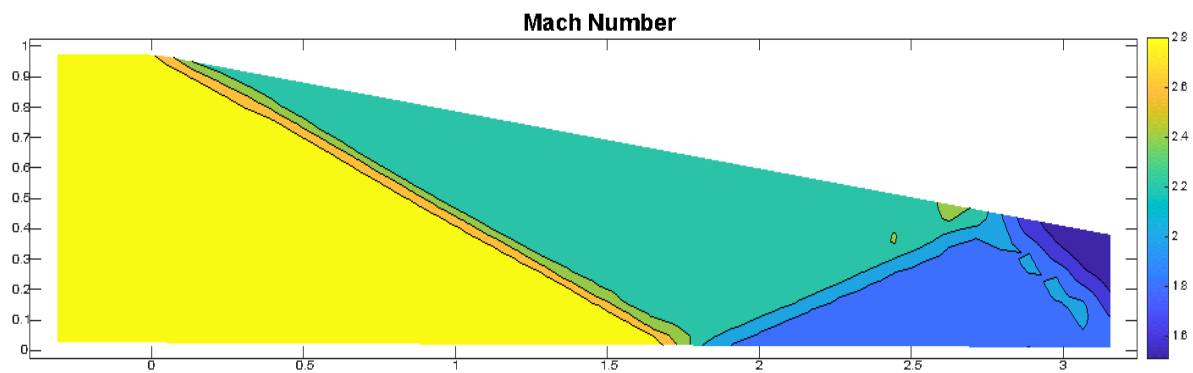
Figure 9 – Contour plot for pressure at IL = 42, JL = 22

Figure 10 – Contour plot for density at IL = 82, JL = 42

Figure 11 – Contour plot for density at IL = 162, JL = 42

Figure 12 – Contour plot for Mach Number at
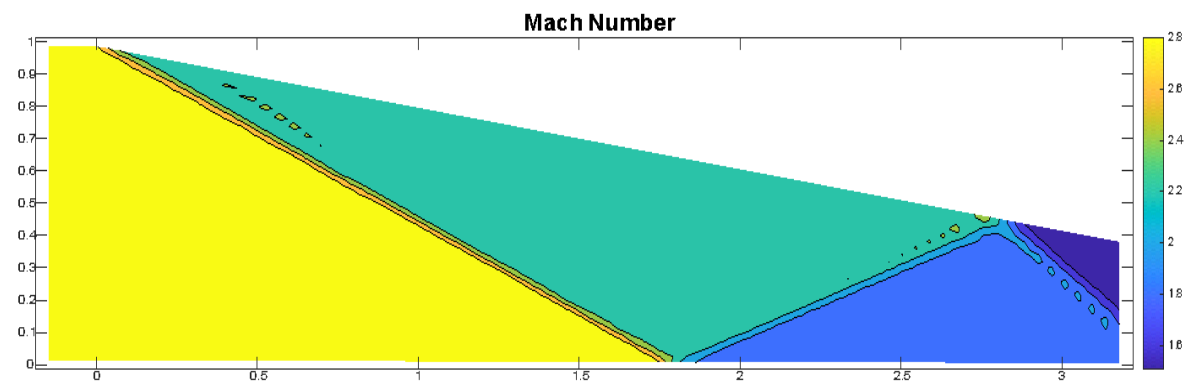
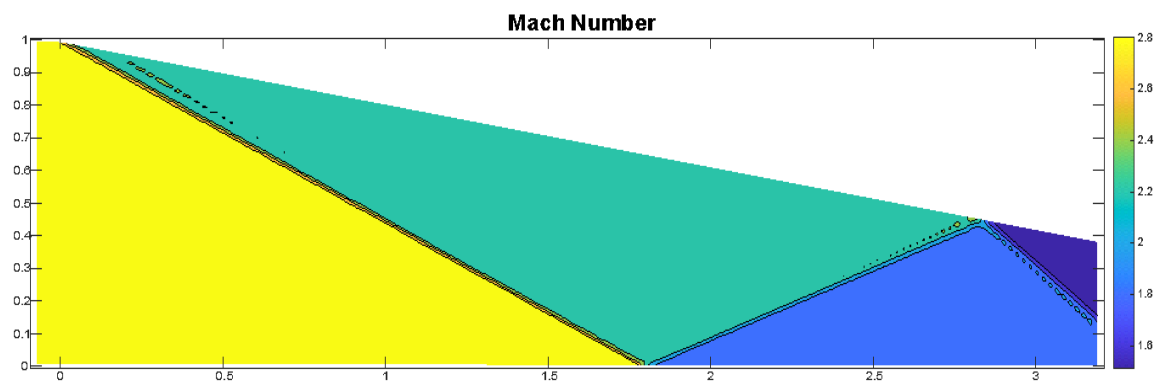Figure 13 – Contour plot for Mach Number at IL = 82, JL = 42

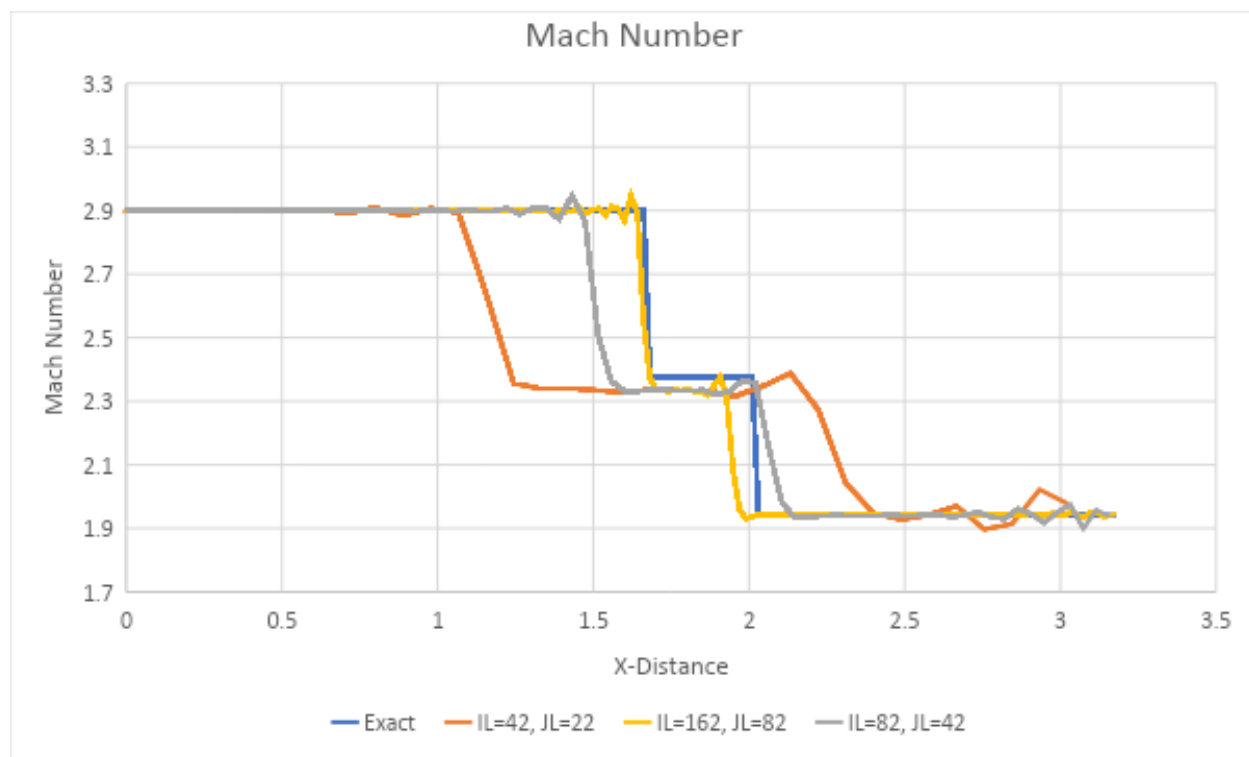Figure 14 – Contour plot for Mach Number at IL = 162, 82
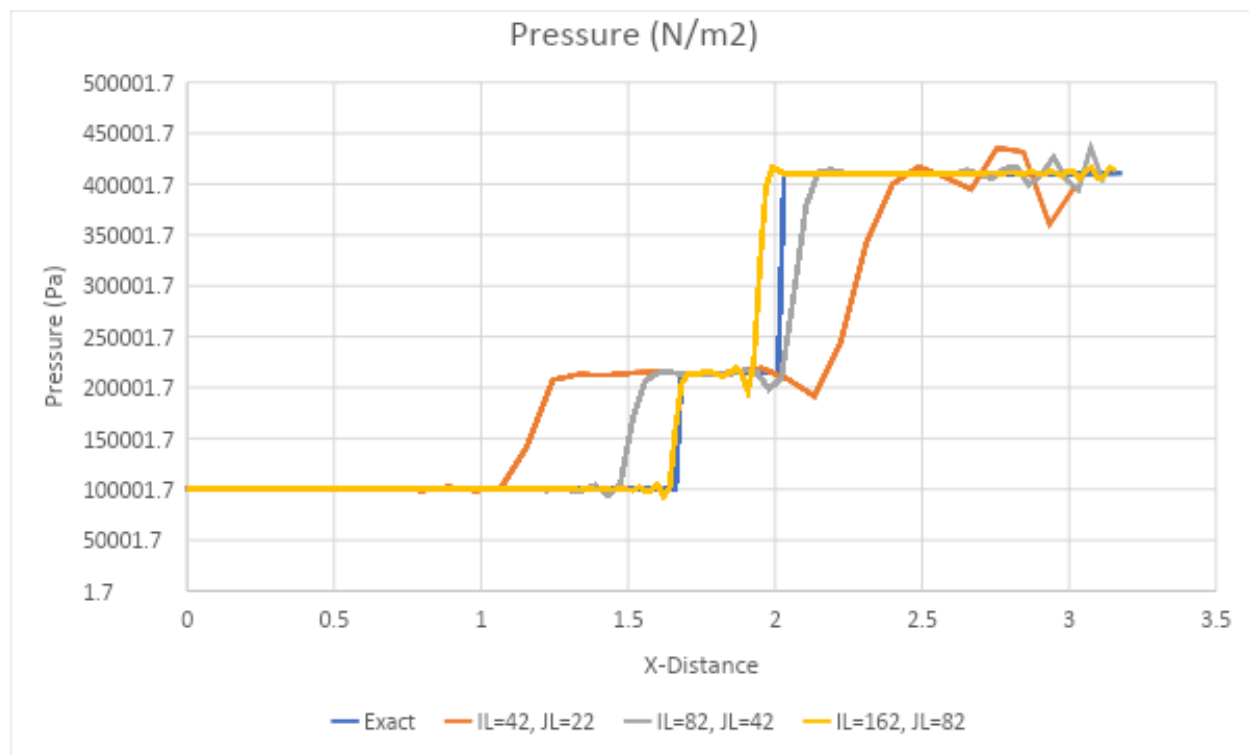
Figure 14 - Mach number along line y = 0.5 m
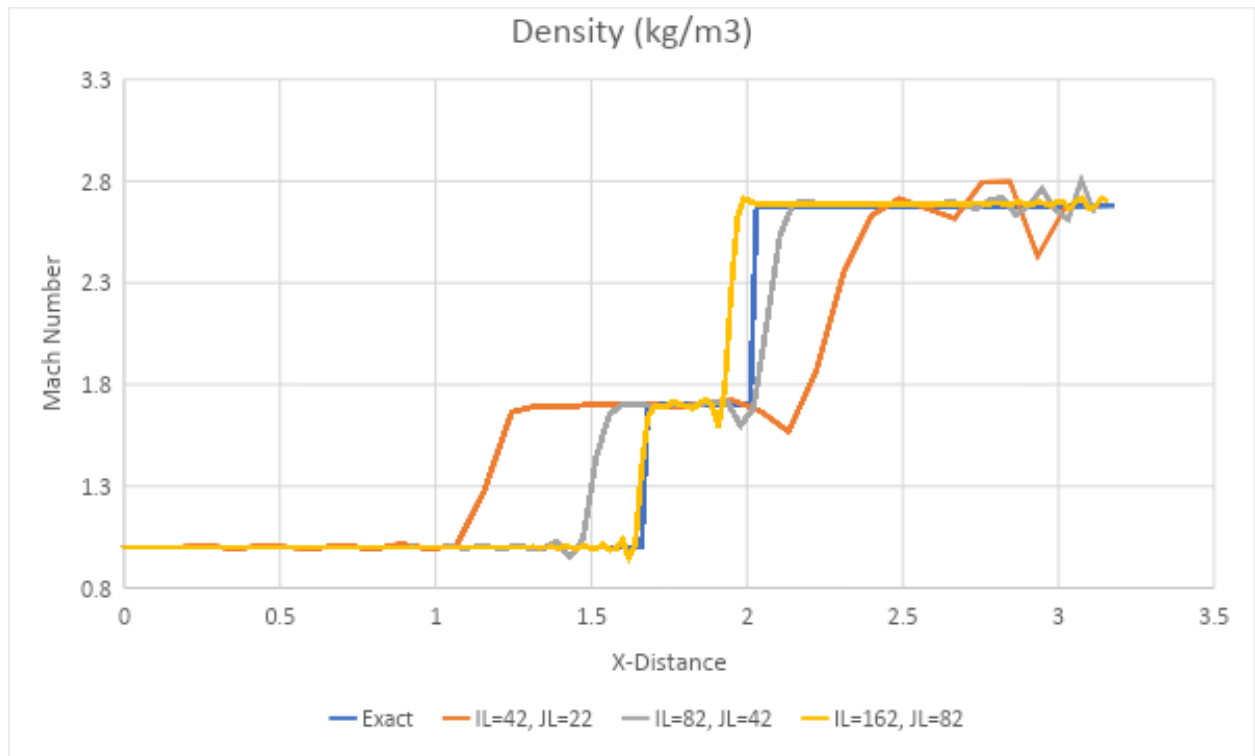
Figure 15 - Pressure number along line y = 0.5 m

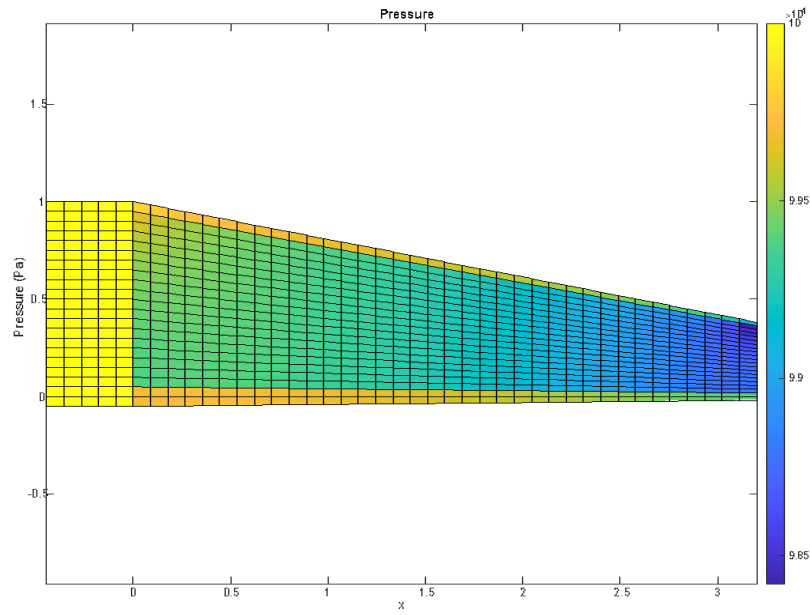Figure 16 - Density number along line y = 0.5 m

Figure 17 – Pressure contour plot for SW Scheme. IL = 42, JL = 22.
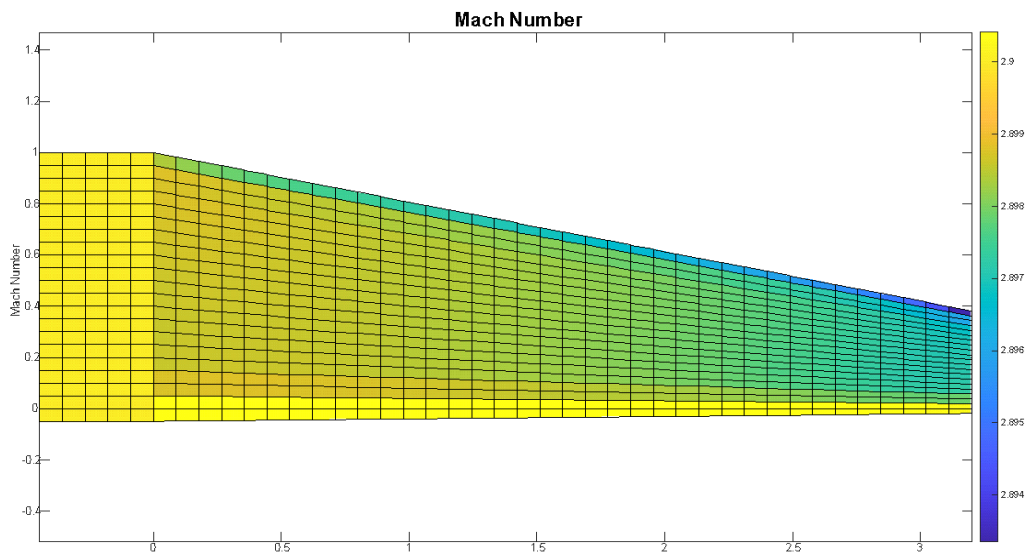

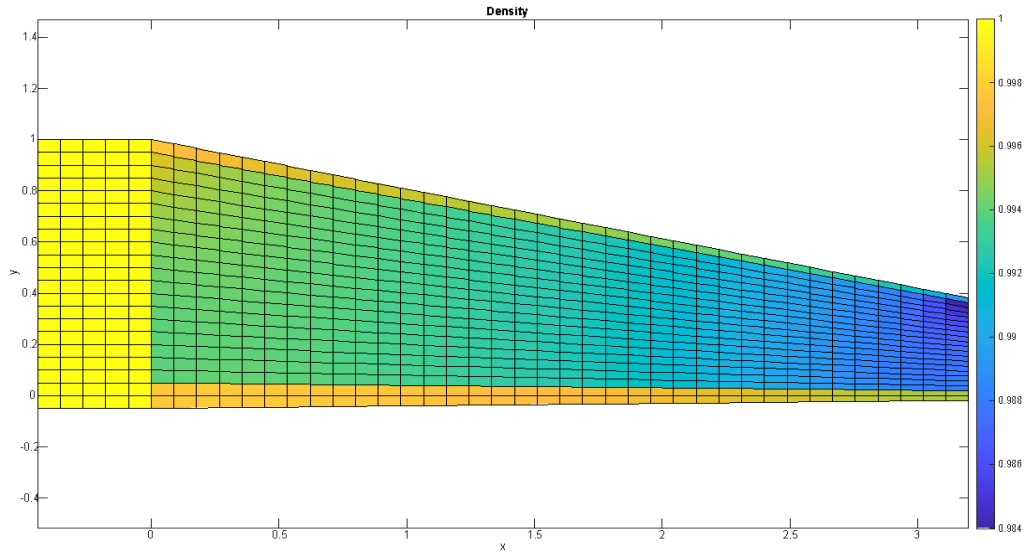Figure 18 – Mach Number contour plots for SW Scheme. IL = 42, JL = 22.

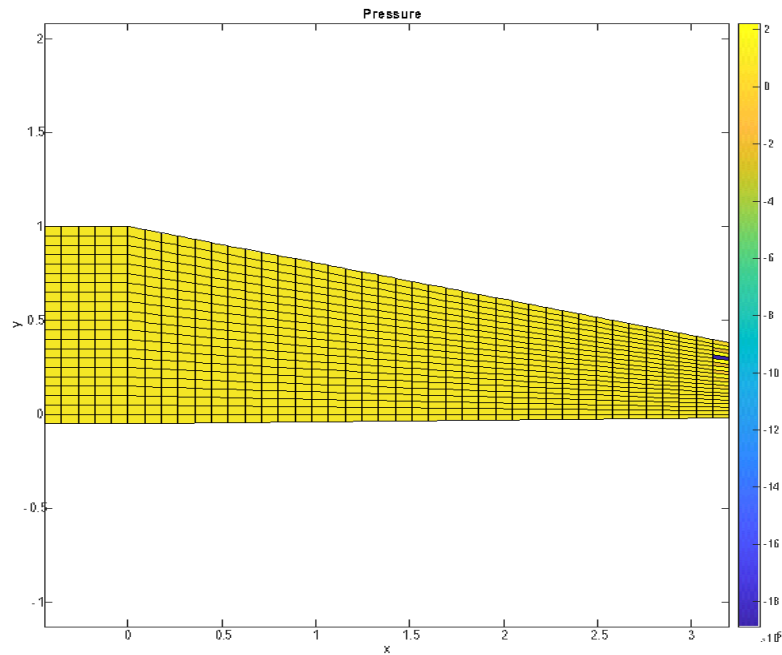Figure 19 – Density contour plots for SW scheme. IL= 42, JL = 42.

Figure 20 – Pressure contour for Roe scheme. IL = 42, JL = 22

Figures 17-19 should serve no other function than additional debugging information. As far as potential root causes, one notable distinction between my plots and the sample code is there is a half cell stagger when I overlay my contour plots over the grid cell. This is illustrated in Figures 21 and 22. There are also additional slave cells around the perimeter of the sample code overlay.
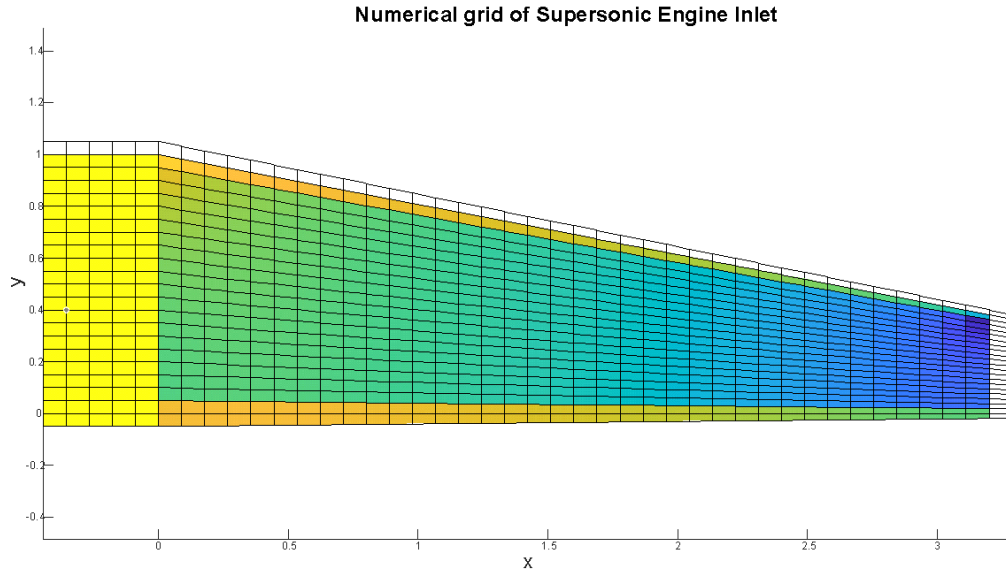
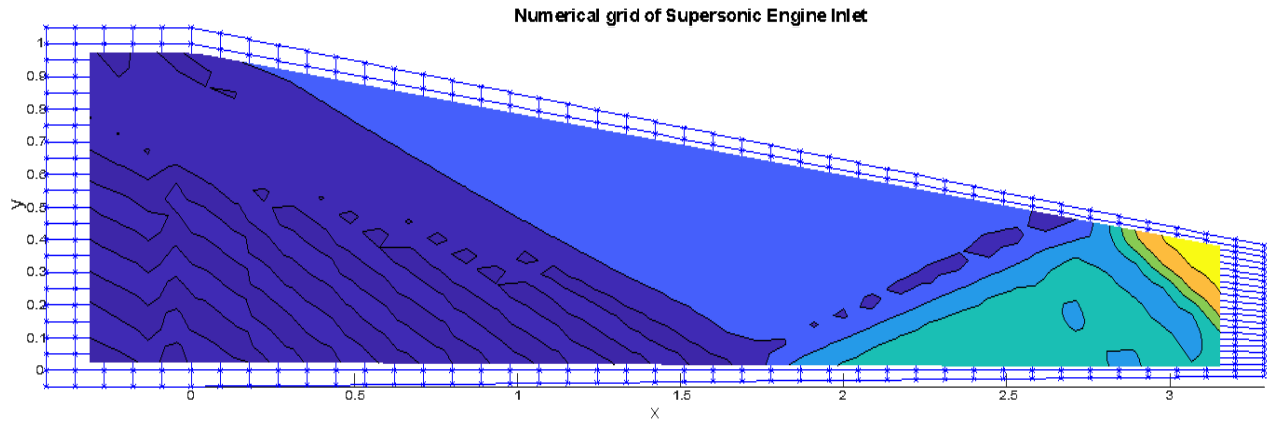Figure 22 – S-W scheme superimposed over grid.

Figure 23 – MacCormack scheme superimposed over grid.

My next steps for debugging my code will be to review the indexing of each scheme and how the upwinding procedure is applied. I will then determine why there is a half cell offset between the two codes.

Section 8 Discussion

Intuitively, we see that the contour plots accurately agree with our theoretical understanding of the behavior of flow properties across shocks. Looking at the Mach Number across the domain, we see that the flow velocity slows down as the pressure increases. Practical uses for this

situation would be the inlet of a ramjet where the high pressures at the exit can assist with a more complete combustion.

Our contour plots that the MacCormack Scheme is very capable of resolving the 2D Euler equation even at coarser grid densities. We see that even at the 42x22 course grid, we can easily distinguish the shock waves and

As expected, our results show that our results converge to the exact solution at finer grid densities. The efficacy of increasing the grid density is clearly illustrated at the oblique shock interface. If we compare the Mach number (Figures 12, 13, and 14) transition of the first oblique shock between the three different grid densities we can see there is a more gradual, dissipative transition at the course grid. The visual indication for this is the width of the orange band between the yellow (State 1) and green (State 2) regions.

This is further illustrated on the plots in Figures 14, 15, and 16. For these three plots, the Mach Number, Pressure, and Density were plotted at y=0.5 m. This corresponds to the middle of the supersonic inlet. When we compare each grid density to the exact solution it becomes very clear that there is a drastic improvement in solution convergence at the higher densities. Another point of interest is the presence of oscillations for the course (42x22) grid near the end of the domain. Typically, oscillations occur at points of sharp discontinuities such as the transition before and after a shockwave, but the coarseness of the grid prevents the CFD code from accurately resolving the flow conditions.

Section 9 Conclusion

From our testing, we can see that using 2-D discretization schemes such as the MacCormack method we are able to accurately determine the flow properties of a 2D domain. The degree of accuracy is determined by the grid density. At the highest grid density, we observe a near convergence to the exact solution. At the course grid densities, we observe oscillations at discontinuities and the inability to accurately capture shocks. Further testing can be done with other CFD schemes that have higher numerical dissipation at discontinuities. These include but are not limited to TVD, ENO, MUSCL (Monotone Upstream-Centered Schemes for Conservation Law), and WENO schemes.

Section 10 References

1. Computational Fluid Mechanics and Heat Transfer by Anderson, Dale Pletcher, Richard H. Tannehill, John C
2. https://www.researchgate.net/publication/273693154_Investigation_and_Improvement_of_Thermal_Efficiency_of_Hypersonic_Scramjet/figures?lo=1&utm_source=google&utm_medium=organic